Decay of $^{58}Co^{m}$

K. J. Moody, N. Gharibyan,* P. M. Grant, D. A. Shaughnessy, J. D. Despotopulos, S. J. Tumey, and T. A. Brown
Physical and Life Sciences Directorate, Lawrence Livermore National Laboratory, Livermore, California 94551, USA

(Received 25 September 2018; published 6 March 2019)

We have studied some of the nuclear decay properties of $^{58}Co^{m}$. The half-life is found to be (8.853 ± 0.023) hours, which is significantly different from the evaluations found in the literature. The absolute intensity of the 24.9-keV γ ray emitted in the internal transition decay is $(0.0387 \pm 0.0016)\%$, in agreement with the calculated yield of a transition of $M3$ multipolarity. We observe γ-ray photons from a previously unreported branch for electron capture decay, with an intensity of $(0.00120 \pm 0.00005)\%$, consistent with expectations from the calculation of log ft.

DOI: 10.1103/PhysRevC.99.034307

I. INTRODUCTION

The ^{58}Co nucleus has two long-lived isomeric states [1], formed by the parallel and antiparallel coupling of $\pi f_{7/2}$ and $\nu p_{3/2}$ single-particle states [2,3]. The $J^{\pi} = 5^{+}$ metastable state decays with a half-life of approximately 9 h to the 71-d $J^{\pi} = 2^{+}$ ground state [4] via a highly converted 25-keV internal transition [5–7] of multipolarity $M3$ [8,9]. $^{58}Co^{m}$ is used in nuclear medicine for the radiotherapy of small tumors [10–12]. The Auger electrons accompanying the internal conversion of the 25-keV transition [13] provide a means of delivering a high radiation dose to gram-size tumors. Improved knowledge of the decay properties of $^{58}Co^{m}$ will allow better calculation of local dosimetry [14].

The ^{58}Ni(n, p) and ^{59}Co$(n, 2n)$ reactions produce the shielded (protected from β decay by stable isobars) nuclide ^{58}Co with distinctly different isomer ratios [15], which could be used as a potential nuclear-forensic fingerprint in debris arising in a thermonuclear detonation. Since the decay of $^{58}Co^{m}$ is difficult to observe directly, its concentration in an experimental sample is often measured indirectly through the ingrowth and subsequent decay of the ground state [15–18]. The accuracy with which the concentration of $^{58}Co^{m}$ can be determined indirectly is dependent, in part, on the accuracy with which its decay half-life is known. We recently performed experiments at the National Ignition Facility with the purpose of measuring the $^{58}Co^{m}/^{58}Co^{g}$ isomer ratio arising from the ^{59}Co$(n, 2n)$ and ^{58}Ni(n, p) reactions at 14 MeV. In following the ingrowth of $^{58}Co^{g}$, we observed that the best fits to the decay curves were obtained with a $^{58}Co^{m}$ half-life that is significantly less than the currently accepted evaluation, (9.10 ± 0.09) h [19]. To improve our isomer-ratio measurements we performed a separate radiochemical experiment to determine the decay properties of $^{58}Co^{m}$.

Sources of $^{58}Co^{m,g}$ were produced in the ^{55}Mn(α, n) reaction [5,20–22]. The angular momentum introduced by the projectile results in enhanced production of the high-spin isomer, providing a more favorable isomer ratio than that produced from reactions with lighter projectiles [16,17,23–25]. In this paper, the $^{58}Co^{m}$ half-life is reported from both direct measurements, from the decay of the 25-keV photon intensity, and indirect measurements, from the ingrowth and subsequent decay of $^{58}Co^{g}$. We also remeasured the decay intensity of the 25-keV photon emitted in the internal transition of $^{58}Co^{m}$ and observed for the first time a small branch for its electron capture (EC) decay.

II. EXPERIMENTAL

The ^{55}Mn target was prepared by mixing powdered Mn metal with powdered Al metal in equal amounts (by weight), and grinding the mixture in a quartz mortar. Approximately 25 mg of the resultant powder was transferred into a 5-mm-diameter die and compressed into a pellet by applying two tons of pressure with a manual hydraulic press. The resulting target behaved like a metal foil, and did not shed activity after irradiation.

To produce $^{58}Co^{m}$, we irradiated the manganese target with ^{4}He ions accelerated with the tandem van de Graaf at the Center for Accelerator Mass Spectrometry (CAMS) [26], at the Lawrence Livermore National Laboratory. The ^{4}He ions [27] were accelerated to an energy of 27 MeV, focused to the diameter of the target and delivered to a stack of foils bolted to a water-cooled beam stop [28]. The Mn target was mounted behind a Pt isotope-production target and thin Al foils [29]. The intervening experiment reduced the beam energy incident on the Mn target to 12.9 MeV [30,31], which is the threshold for the onset of the ^{55}Mn$(\alpha, 2n)^{57}$Co reaction [32]. The small amount of ^{57}Co observed in the irradiated sample arose through broadening of the beam energy profile in the leading foils, along with minor deviations from homogeneity in their areal densities. The Mn target was sufficiently thick that the beam stopped in the target [30]. The nominal beam intensity was 300 pnA (1.9×10^{12} particles/sec), and the duration of the irradiation was 3 h.

*Corresponding author: gharibyan1@llnl.gov

Following irradiation, the foil stack was transported to the radiochemistry facility, where the Mn target was available for processing 30 min postirradiation. The target was dissolved [33] in 0.5 ml 6 M HCl, added dropwise, then heated to complete dissolution. The resulting solution was diluted to 1.5 ml with addition of concentrated HCl, and after mixing was passed through a 4-mm-diameter anion-exchange column (AG 1-x8 resin, 140 mesh), preconditioned with 9 M HCl. The column eluent from the original solution and 5 ml of 9 M HCl column wash (containing Al and Mn) was set aside. Co was then eluted from the column with 2 ml of 2 M HCl, and the chemical fraction was evaporated to a small volume. The overall chemical yield of the procedure was (98.5 ± 1.0)%, based on the measurement of side fractions. The sample was split into two parts, with both solutions evaporated to dryness in 1-cm^2 spots on Pt foils and then heated to an orange glow in a Bunsen burner flame. The final counting sources were adherent and contained no visible contaminating mass. The sources were available for counting 2 h after the end of the irradiation.

γ-ray intensities were measured with HPGe semiconductor detectors [34]. Spectral data were acquired as singles using standard counting electronics. The detectors were calibrated for energy and efficiency responses with a set of radionuclide standards, including commercial mixed-radionuclide sources traceable to NIST as well as locally produced single-nuclide sources (including ^{152}Eu, ^{241}Am, and ^{140}Ba) [35–37]. The efficiency functions derive from a geometrical model based on the construction of the detectors, benchmarked against the calibration sources. Spectral data were collected as time-tagged histograms in 4096 channels. For COAX detectors, photon events between 50 keV and 2 MeV were collected; for LEPS detectors, photon events between 10 keV and 400 keV were collected. Samples were mounted in fixtures at well-defined locations (±0.02 cm), coaxial with the detectors, and were not moved during the acquisition of the decay-curve data. Detectors were shielded with at least 5 cm of lead, lined with cadmium and copper to reduce the detection of the fluorescence of lead.

One sample (CO-3) contained 83% of the final Co product and was counted 8 cm from the window of a germanium LEPS detector. A 0.5-mm-thick Al absorber covered the sample to attenuate electrons and very-low-energy photons, reducing the relative rate of summing events. Electronic dead time, which increased over the course of the experiment due to the contribution of the ingrowth of ^{58}Co^g to the continuum at low energy, did not exceed 2%. The decay of the intensity of the 24.9-keV γ-ray was followed for 4 d with data accumulated every 3 h.

The second sample (CO-4) contained 17% of the final Co product and was mounted 4 cm from the window of a 12% COAX detector. A 480 mg/cm^2 Cd absorber covered the sample to attenuate low-energy photons. Electronic dead time did not exceed 3% over the course of the experiment. The ingrowth of the intensity of the 811-keV γ ray from ^{58}Co^g decay was followed for 0.5 day with data accumulated every 70 min, then for another 3.5 d with progressively larger acquisition intervals as the effect of ^{58}Co^m decay on that of ^{58}Co^g was reduced.

TABLE I. Nuclear data [19,37] used in the cross calibration of the two detectors and in the calculation of the isotope inventory at end of irradiation. Uncertainties (1-σ) on the last digit(s) are given in parentheses.

Nuclide	Half-life (d)	Photon energy (keV)	Photon intensity (%)
^{57}Co	271.79(9)	14.41	9.16(15)
		122.06	85.60(17)
		136.47	10.68(8)
		692.0	0.157(9)
^{58}Co^g	70.86(6)	810.8	99.45(1)
		864.0	0.69(1)
		1674.7	0.52(1)

Following the initial 4 d of counting, both samples were counted with each of the two detectors, with the samples mounted at 15 cm from the detector faces, for cross calibration. The long-lived nuclides ^{57}Co and ^{58}Co^g were used for these measurements. It was found that a systematic discrepancy of 2.5% existed between the efficiency functions of the two detectors. All of the data reported below are corrected (with appropriate propagation of uncertainty) to the basis of the COAX detector for samples at 15 cm. This correction is critical to the calculation of the absolute intensity of the 24.9-keV photon, discussed in Sec. III C.

Photon spectra were processed with the GAMANAL code [38,39]. Spectral peak shapes as a function of photon energy were used in the quantification of photopeak areas, the resolution of doublets, and the calculation of peak-energy centroids. The code integrates peaks over an extrapolated continuum, applies energy and efficiency calibration functions, makes a geometrical adjustment for the finite extent of the source deposits, and calculates the effects of attenuation by the interposed Al and Cd absorber foils [40,41]. Half-thicknesses for the absorbing materials have associated uncertainties of approximately 2% [42], which is included in the propagation of uncertainty of the photopeak intensities. The code also subtracts the contribution of detector background to each photopeak, measured in a separate long count without a source present.

Nuclear data associated with the decay of selected cobalt nuclides [19,37] are given in Table I. These data were used in the cross calibration of the two detectors. They were also used in the calculation of the postirradiation isotope inventory listed in Table II.

III. RESULTS

A. γ-ray spectra of Co isotopes

In Fig. 1, sections of two γ-ray spectra from the more radioactive sample (CO-3) are shown, the first and thirtieth 3-h counts taken with a LEPS detector. The later spectrum is scaled downward by a factor of 0.1. In the 3.67 d that elapsed between the two counts, the dominant 24.9-keV γ-ray associated with the IT of 9-h ^{58}Co^m decayed to undetectable levels. At higher energies than shown, the two most intense γ rays arising in the decay of 272-day ^{57}Co were readily visible. The strong ^{57}Co γ line at 14.4 keV is barely visible in the

TABLE II. Isotope production in the cobalt fraction produced by the irradiation. The nuclide inventory is the sum from samples CO-3 and CO-4, comprising (98.5 ± 1.0)% of the cobalt product. The $^{58}Co^{m+g}$ activity was calculated by extrapolating the asymptotic $^{58}Co^{g}$ activity backwards in time to the end of the irradiation.

Nuclide	Atoms at end of irradiation
^{57}Co	$1.79 \times 10^{10} \pm 2\%$
$^{58}Co^{m+g}$	$8.74 \times 10^{11} \pm 2\%$
^{61}Cu	$2.0 \times 10^{7} \pm 10\%$

later spectrum, partly due to the interposed Al absorber; while 137 mg/cm^2 of Al attenuates the intensity of the 24.9-keV photon by only 16%, the 14.4-keV photon is attenuated by 58% [40].

In Fig. 2, a section of a γ-ray spectrum from the less radioactive sample (CO-4) is shown; it is the first 70-min count taken with a COAX HPGe detector, with a temporal midpoint 0.11 d after irradiation. The spectrum is dominated by radiation arising from the EC/β^+ decay of $^{58}Co^{g}$, along with an easily visible contribution from the decay of ^{57}Co. The small peak at 1322 keV is due to summing of annihilation radiation with the 810.8-keV photon [43]. The cobalt fraction was radiochemically pure, other than a very small contribution from 3.4-h ^{61}Cu [44]. The ^{61}Cu activity likely arose from irradiation of contaminants introduced by the steel dies used in pressing the target foil, and was incompletely removed by the radiochemical procedure [45].

The isotopic content of the initial radiochemical fraction used to produce the two counting sources, decay corrected to the end-of-irradiation time, is given in Table II. The ^{57}Co and $^{58}Co^{m+g}$ data were calculated using the information in Table I; ^{61}Cu was calculated from literature data [37]. The $^{58}Co^{m+g}$ value was determined by extrapolating the $^{58}Co^{g}$ intensity data taken at late times to the end of irradiation using the $^{58}Co^{g}$ half-life (the asymptotic assumption).

B. Half-life of $^{58}Co^{m}$

The half-life of $^{58}Co^{m}$ can be obtained from the sequence of counts taken with the LEPS detector from sample CO-3 (see Fig. 1). The 24.9-keV photopeak intensity is plotted as a function of time-after-irradiation in Fig. 3. Since the dead time associated with data acquisition was small (<2%) and the live time of each counting interval was the same, no corrections were made for the nonlinearity of the decay intensity within each counting interval, which should be the same for each data point. The sample was placed at a fixed location for the duration of the acquisition of the decay curve, so uncertainties associated with the efficiency calibration became systematic and were not included in the error bars. As the $^{58}Co^{m}$ signal decayed with time, any error in the calculation of the subtracted continuum had an increasing effect on the residual photopeak areas and, consequently, the calculation of the half-life. The continuum under the 24.9-keV photopeak arises primarily from the decay of $^{58}Co^{g}$ and is nearly constant across the relevant energy region (Fig. 1). Consequently, the subtraction of the continuum from the gross peak areas was assumed to be executed properly in the GAMANAL analysis and should not bias the half-life determination [46].

The single-component decay-curve analysis was performed with a nonlinear least-squares code [47,48]. The data measured for Fig. 3 cover more than nine analyte half-life

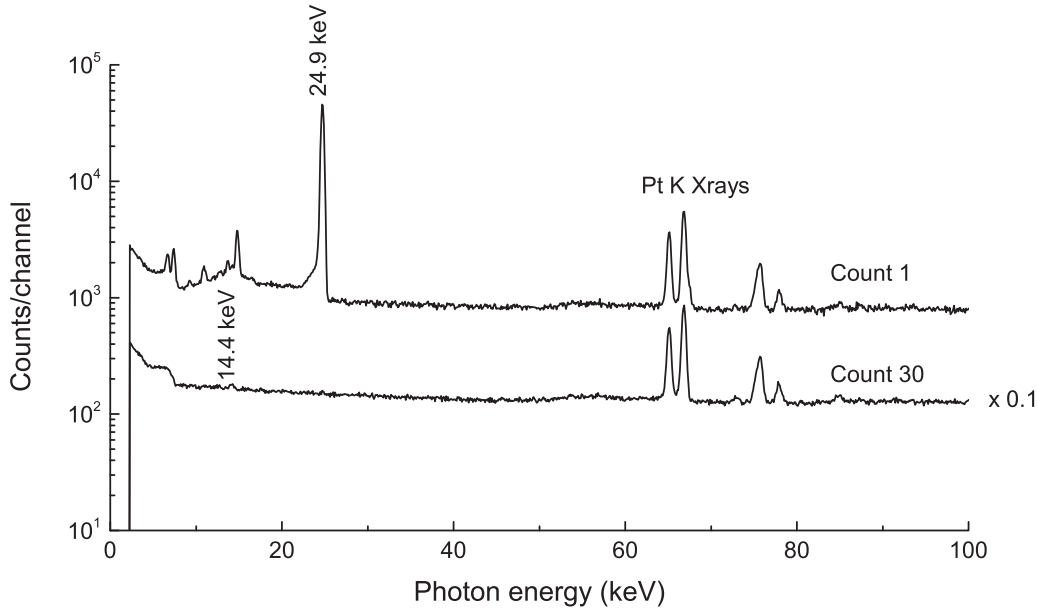

FIG. 1. Sections of two γ-ray spectra of 3-h duration, from sample CO-3, taken with a LEPS detector. The midpoint times of the acquisition intervals were 0.15 and 3.82 d after irradiation. The later count is scaled by a factor of 0.1. The main features of the spectra are the 24.9-keV photon associated with $^{58}Co^{m}$ decay and the Pt K x rays from fluorescence of the sample substrate, induced mainly by radiation from the decay of $^{58}Co^{g}$.

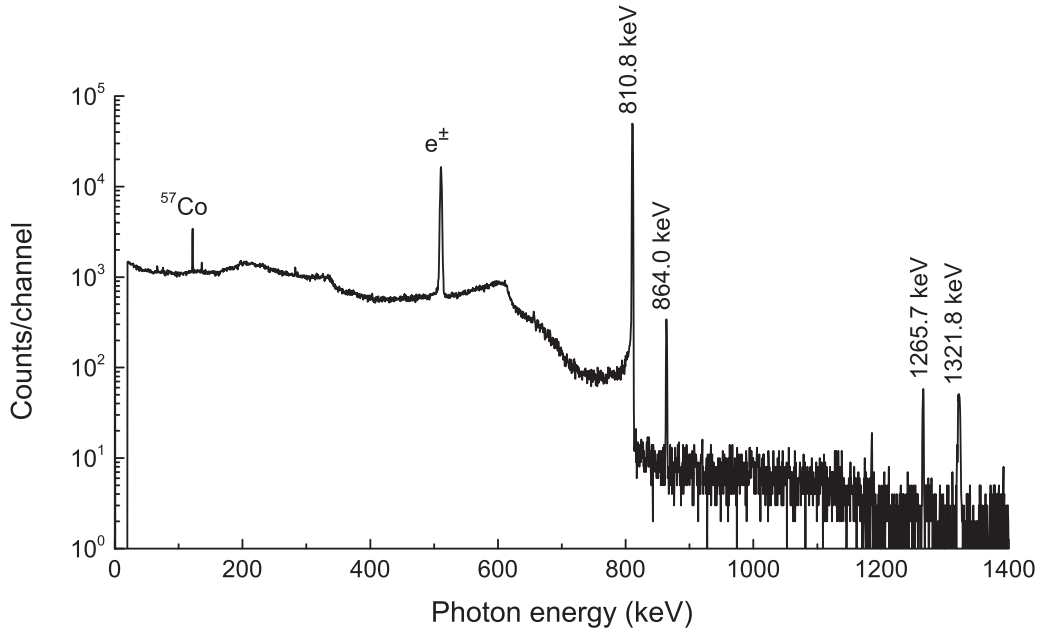

FIG. 2. A section of the first 70-minute γ-ray spectrum of sample CO-4, taken with a COAX HPGe detector. The midpoint of the acquisition interval was 0.11 day after irradiation. The main features of the spectrum are the photon lines associated with the decays of ^{57}Co and ^{58}Co^{g}, and the annihilation peak at 511 keV. The peak at 1322 keV is due to summing of annihilation radiation with the 810.8-keV photon from ^{58}Co^{g} decay. The 1265.7-keV peak, decaying with a 9-hr half-life, is discussed in the text.

periods, resulting in a well-constrained fit, shown as a solid line in the figure. The half-life of ^{58}Co^{m} from the direct measurement of the 24.9-keV photon decay is (8.847 ± 0.023) hours, a significant departure from the literature (see Sec. IV). The error bar is one σ.

The half-life of ^{58}Co^{m} can also be obtained from the sequence of counts taken with the COAX detector from sample CO-4 (Fig. 2). The 810.8-keV photopeak intensity from the EC/β^{+} decay of ^{58}Co^{g} [49–51] is plotted as a function of time after irradiation in Fig. 4. The ingrowth of ^{58}Co^{g} from the decay of ^{58}Co^{m} is easily observed at early times. The nonlinearity of photon intensity across the counting interval can be important when constructing a decay curve for an activity that is growing into a sample. To minimize this effect

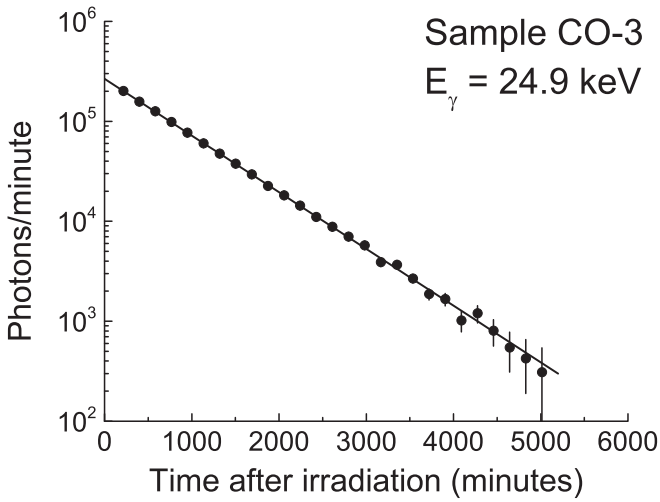

FIG. 3. The decay curve constructed from the 24.9-keV photopeak data taken with the LEPS detector (Fig. 1). Vertical one-σ error bars on the data points are smaller than the size of the markers unless explicitly shown. Data are consistent with a ^{58}Co^{m} half-life of (8.847 ± 0.023) hours. The weighted least-squares fit to the data is shown as a solid line.

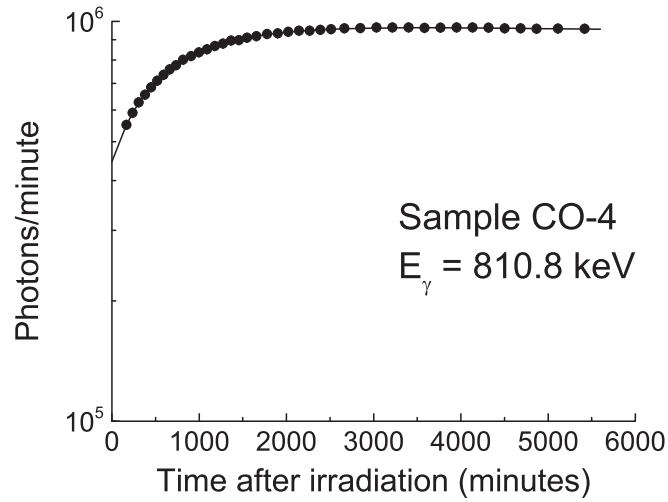

FIG. 4. The decay curve constructed from the 810.8-keV photopeak data taken with the COAX HPGe detector (Fig. 2). Vertical one-σ error bars on the data points are smaller than the markers. Holding the half-life of ^{58}Co^{g} fixed at 70.86 days, a least-squares fit of a growth-and-decay function to the data (solid line) is consistent with a ^{58}Co^{m} half-life of (8.942 ± 0.070) h.

we selected an initial counting interval that was short (70 min) compared to the half-life of the parent activity (9 h). As $^{58}Co^{m}$ decayed and the decay rate of the 810.8-keV photopeak became increasingly dominated by the half-life of $^{58}Co^{g}$, the counting intervals became longer. As before, the sample was placed in a fixed location for the duration of the decay-curve measurements, allowing exclusion of uncertainties associated with the efficiency calibration from the error bars. The 810.8-keV signal changed by only a factor of 2 over the course of the measurements, so the subtraction of the relatively small continuum, mostly arising from higher-energy photon transitions from $^{58}Co^{g}$ decay, was not expected to bias the interpretation of the decay curve.

The decay curve shown in Fig. 4 was fit with a growth-and-decay function [47,48], shown as a solid line. The literature evaluation of the $^{58}Co^{g}$ half-life is based on a large number of experimental determinations that are in good agreement, so we held its half-life fixed at 70.86 d in the calculation [19,52]. The half-life of $^{58}Co^{m}$ from the indirect measurement of the ingrowth of the 810.8-keV photopeak is (8.942 ± 0.070) h, in reasonable agreement with the direct determination through the decay of the 24.9-keV photon, given above. The error bar is also one σ.

The best value for the half-life of $^{58}Co^{m}$ is a weighted average of the two measurements, (8.853 ± 0.023) h. This is consistent with our less precise determinations of the half-life arising from experiments at the National Ignition Facility (Sec. I).

C. Absolute intensity of the 24.9-keV photon

The γ-ray spectra obtained from samples CO-3 and CO-4 provide the basis for calculating the absolute intensity of the 24.9-keV photon emitted in the decay of $^{58}Co^{m}$.

Analysis of the decay curve shown in Fig. 4 results in a value for $[^{58}Co^{m}]/([^{58}Co^{m}] + [^{58}Co^{g}])$ of (0.5496 ± 0.0055) at the end of irradiation. A count of CO-3 on the COAX detector, long after $^{58}Co^{m}$ had decayed to unobservable levels, resulted in a measurement of $([^{58}Co^{m}] + [^{58}Co^{g}])_{\text{measurement}}$, which when decayed backwards to the end of irradiation resulted in a value of $([^{58}Co^{m}] + [^{58}Co^{g}])_{\text{asymptotic}}$ of $(7.229 \times 10^{11} \pm 0.4\%)$ atoms. The asymptotic value of $[^{58}Co^{g}]$ that grows in from $^{58}Co^{m}$ is related to the true value by the ratio $(\lambda_m - \lambda_g)/\lambda_m$, where λ_m and λ_g are the decay constants of $^{58}Co^{m}$ and $^{58}Co^{g}$, respectively [53]; this factor is sufficiently close to unity to ignore. Thus, the inventory of $^{58}Co^{m}$ in sample CO-3 at end of irradiation was $(3.973 \times 10^{11} \pm 1.1\%)$ atoms.

Using the half-life of $^{58}Co^{m}$ determined in Sec. III B, the initial activity of $^{58}Co^{m}$ in sample CO-3 was $(5.184 \times 10^{8} \pm 1.1\%)$ disintegrations/min. The analysis of the decay curve shown in Fig. 3 results in the absolute emission rate of the 24.9-keV photon. This value, adjusted slightly downward for the effect of nonlinearity of decay during the 3-h acquisition intervals, corrected for the cross calibration of the LEPS and COAX detectors, and propagated with the uncertainty of the efficiency of the LEPS detector, is $(2.008 \times 10^{5} \pm 4.2\%)$ photons/min. This results in an absolute intensity of the 24.9-keV photon of $(0.0387 \pm 0.0016)\%$, in reasonable agreement with the literature (see below). The error bar is one σ.

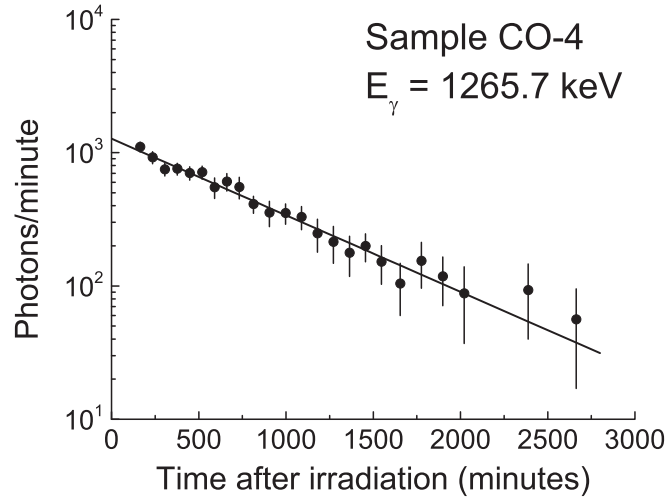

FIG. 5. The decay curve constructed from the 1265.7-keV photopeak data taken with the COAX HPGe detector (Fig. 2). Vertical error bars are one σ. Data are consistent with a half-life of (8.73 ± 0.55) h, supporting an assignment to the decay of $^{58}Co^{m}$. The weighted least-squares fit to the data is shown as a solid line.

D. Radiation emitted in the EC decay of $^{58}Co^{m}$

All photopeaks in the COAX spectra of sample CO-4 (Fig. 2) were assigned to 272-day ^{57}Co, 71-d $^{58}Co^{g}$, or 3.4-h ^{61}Cu, with the exception of the peak at 1266 keV. The weighted average of several determinations of its energy in successive γ-ray spectra resulted in a value of (1265.74 ± 0.07) keV, which closely matches a strong γ transition in the β^- decay of 65-sec $J^{\pi} = 4^{+}$ $^{58}Mn^{m}$ [19,54] to states in ^{58}Fe, (1265.74 ± 0.05) keV [55,56]. The $J^{\pi} = 4^{+}$ parent state at 2076.5 keV is not populated in the decay of $^{58}Co^{g}$ [19]. Figure 5 shows the decay curve of the 1266-keV photopeak, constructed from the COAX counts of sample CO-4. A single-component decay curve fit to the data (solid line) has a half-life of (8.73 ± 0.55) hours, consistent with the observed half-life of $^{58}Co^{m}$. These observations suggest that the decay of $^{58}Co^{m}$ has a previously unobserved branch for EC decay to states in ^{58}Fe that are also populated in the decay of $^{58}Mn^{m}$.

As discussed above, decay-curve analysis of the 810.8-keV photopeak gave a value of (0.5496 ± 0.0055) for the atom ratio $[^{58}Co^{m}]/([^{58}Co^{m}] + [^{58}Co^{g}])$ at the end of irradiation. For sample CO-4, the asymptotic extrapolation of $[^{58}Co^{g}]$ to end of irradiation yielded $([^{58}Co^{m}] + [^{58}Co^{g}]) = (1.494 \times 10^{11} \pm 0.4\%)$ atoms. Applying the $^{58}Co^{m}$ half-life to the calculated end-of-irradiation atoms of $[^{58}Co^{m}]$ resulted in a value of $(1.072 \times 10^{8} \pm 1.1\%)$ disintegrations/min. Holding the $^{58}Co^{m}$ half-life fixed at 8.853 h and forcing the fit to the decay curve of Fig. 5 gave an initial photon intensity of (1290 ± 44) γ rays/min for the 1266-keV peak. Therefore, the absolute intensity of the 1266-keV γ ray emitted in the EC decay of $^{58}Co^{m}$ is $(0.00120 \pm 0.00005)\%$.

Assuming that the 1266-keV γ ray arises in most of the $^{58}Co^{m}$ EC decays (see below), the EC branch is sufficiently

TABLE III. Reported half-life of $^{58}Co^{m}$.

Half-life (h)	Publication year	Reference
8.8	1950	[5]
9.2 ± 0.2	1950	[57]
9.0 ± 0.2	1952	[24]
9.2 ± 0.2	1952	[58]
9.0 ± 0.2	1960	[15]
9.15 ± 0.10	1967	[8]
9.5 ± 0.5	1968	[9]
9.3 ± 0.3	1968	[59]
8.94 ± 0.17	1970	[6]
8.94 ± 0.17	1973	[60] (Evaluation)
9.15 ± 0.10	1996	[37,61] (Evaluation)
9.04 ± 0.11	1999	[62,63] (Evaluation)
9.10 ± 0.09	2010	[19] (Evaluation)
8.853 ± 0.023	2018	this work

small that it does not impact the calculation of the 24.9-keV photon intensity presented in Sec. III C.

IV. DISCUSSION

A. $^{58}Co^{m}$ half-life compared with the literature

In Sec. III B, we reported the $^{58}Co^{m}$ half-life to be (8.853 ± 0.023) h, significantly less than expectation based on modern evaluations. In Table III, this measurement is compared with the literature, the results of nine measurements and four evaluations. All of the measurements were performed before any of the evaluations. The first four reported values [5,24,57,58] were obtained by following the decay of the gross activity of the experimental samples with Geiger-Muller counters, and only the last two measurements [6,59] employed germanium semiconductor detectors. The last measurement [6], which the 1973 evaluation considered the most reliable [60], is in close agreement with our value.

B. 24.9-keV photon intensity

Our measurement of the absolute intensity of the 24.9-keV photon (Sec. III C) resulted from relating its relative intensity to that of the 810.8-keV photon emitted in the decay of $^{58}Co^{g}$ via application of the decay equations describing the ingrowth of the daughter [53]. The absolute intensity of the 810.8-keV photon is known, tying the relative intensity of the 24.9-keV photon to the absolute decay rate of $^{58}Co^{m}$. Previous measurements of the 24.9-keV intensity were made as byproducts of the determination of the multipolarity of the transition (mostly $M3$) through the measurement of the relative intensities of the γ ray and the K- and L-x rays [6–9,60]. Evaluators assumed that the total transition intensity was divided between the γ ray and x rays, calculating unobserved x-ray intensity based on theory [64]. Both pathways to the absolute γ-ray intensity should give the same answer, but measurement of the low-energy photons characteristic of Co x-ray transitions can potentially suffer from unquantified attenuation due to sample thickness.

TABLE IV. Photon intensity of the 24.9-keV transition.

Absolute intensity	Reference
(0.0369 ± 0.0011)%	[37]
(0.0389 ± 0.0012)%	[62]
(0.0397 ± 0.0006)%	[19]
(0.0387 ± 0.0016)%	this work

In Table IV, three independent evaluations of the 24.9-keV photon intensity are listed. They compare favorably with our measurement, which employed a different method. Although $M3$ character would be expected to dominate a transition between two states with the same primary quantum numbers and a spin change of $\Delta J = 3$, a contribution from the $E4$ multipolarity cannot be excluded from first principles, though consideration of single-particle $B(E4)$ would indicate that the contribution is very small [65]. The sum of the internal conversion coefficients for the K and L shells are 2.48×10^{3} and 1.58×10^{5} for 24.9-keV transitions of $M3$ and $E4$ multipolarity, respectively [64]. Consequently, the photon yield of an $E4$ transition is no greater than 6.3×10^{-4}%, making $E4$ a small contribution at best to the observed process. The ratio of L/M conversion intensities is approximately 7 [7,66,67] and the contribution of the N shell is not expected to be significant [68]. This leads to a total $M3$ conversion coefficient of 2.57×10^{3} and a calculated $M3$ photon intensity of 0.0389%. More modern internal conversion coefficients do less adequately reproduce the results of the experiment [69], but yield a similar $E4/M3$ value. The agreement with the data in Table IV supports the more accurate interpretations obtained from the x-ray intensities; the 24.9-keV IT transition is of $M3$ multipolarity with very little $E4$ character [7,8,60,66].

C. EC branch of $^{58}Co^{m}$ decay

Figure 6 depicts the mass-chain decay scheme information for $^{58}Co^{m}$ and its potential decay daughters. The pairing gap in even-even ^{58}Ni ensures that only one state is energetically accessible to accept β^{-} decay from $^{58}Co^{m}$, and the $\Delta J = 5$ spin change makes such decays very unlikely. The level scheme of ^{58}Fe below 3 MeV is well studied, from the 6.25-MeV β^{-} decay of $^{58}Mn^{m}$ [56] and from particle scattering experiments [70,71]. The one-to-one correspondence between the experimental level scheme and the states calculated with the shell model [72,73] makes it improbable that there are unknown states in ^{58}Fe at low excitation energies. Only five states in ^{58}Fe are energetically accessible to the EC decay of $^{58}Co^{m}$ [19], as shown in Fig. 6.

In Table V, we outline a log ft calculation of the approximate partial half-lives for $^{58}Co^{m}$ decays to the indicated states. The log f values were interpolated from tabular data [74]. The expected range of log ft values [53] is an expression of the degree of understanding of the effects of nuclear structure on β-decay processes [75].

From Table V, we would argue that essentially all of the EC decay of $^{58}Co^{m}$ populates the 2077-keV state in ^{58}Fe. Only two states at lower excitation energy can receive low-multipolarity γ transitions, the 2^{+} states at 811 keV and

TABLE V. Expected transition rates to states in the daughter nuclei, in the β^- and EC/β^+ decay of $J^\pi = 5^+$ $^{58}Co^{m}$.

Daughter nuclide	Excitation energy (keV)	J^π	Transition type	Expected range, log ft	Q_{β^-} (keV)	Q_{EC} (keV)	log f	Partial half-life
^{58}Ni	0	0^+	fourth forbidden unique	>23	407		−0.40	$>10^{15}$ yr
^{58}Fe	0	0^+	fourth forbidden unique	>23		2332	1.89	$>10^{13}$ yr
^{58}Fe	811	2^+	second forbidden unique	13–18		1521	0.82	10^4–10^9 yr
^{58}Fe	1675	2^+	second forbidden unique	13–18		657	−0.66	10^6–10^{11} yr
^{58}Fe	2077	4^+	allowed, ℓ-forbidden	6–12		255	−1.71	1–10^6 yr
^{58}Fe	2134	3^+	second forbidden	11–15		198	−1.95	10^5–10^9 yr

1675 keV (Fig. 6). Only the 1266-keV photon is observed in the depopulation of the 2077-keV state [19,37]. If we assume a single-particle model, the relative population rates of the two states go as E_γ^5 [76], so that the state at 811 keV is populated with 300 times the intensity as the 1675-keV state. The 811-keV and 2077-keV states are both members of the ground-state rotational band, which also favors γ decay to the 811-keV state. The γ transition is of $E2$ multipolarity and is expected to undergo internal conversion at a low rate, <0.1% [67]. These observations lead to the conclusion that the intensity of the 1266-keV γ ray is approximately equal to the $^{58}Co^{m}$ EC rate.

The 1266-keV photon intensity is $(0.00120 \pm 0.00005)\%$ of the total decay rate of $^{58}Co^{m}$ (Sec. III D); by the argument above, this is also the EC branch. Given the total half-life for $^{58}Co^{m}$ decay (Sec. III B), the partial half-life for EC decay is 84 years, or a log t of 9.42. From Table V, this results in a log ft of 7.71, in the expected range for an allowed, ℓ-forbidden, transition to the 2077-keV state.

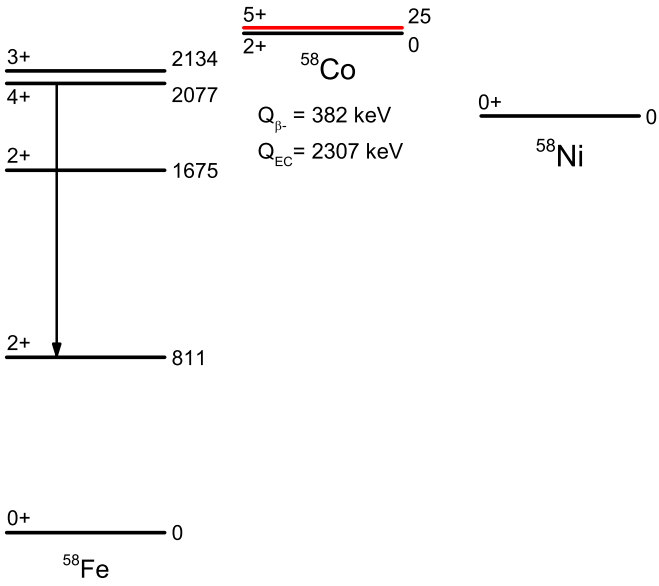

FIG. 6. Mass-chain decay scheme information for $A = 58$. Only the ground state of ^{58}Ni is energetically accessible to potential β^- decay from $^{58}Co^{m}$, but five states of ^{58}Fe are accessible to potential EC/β^+ decays. The observed γ transition is placed in the ^{58}Fe level scheme. The γ transition depopulating the 811-keV state, which also arises in the decay of $^{58}Co^{g}$, is not shown.

From Fig. 6, the 1266-keV γ transition is followed immediately by a 811-keV $E2$ γ transition. Both transitions have photon yields of nearly 100% [67], so the intensity of the 811-keV photon emitted in $^{58}Co^{m}$ EC decay is nearly equal to that of the 1266-keV photon. Of course, the radiation is obscured in the singles spectrum by the overwhelming photon intensity of 811-keV photons arising in the EC decay of $^{58}Co^{g}$. In principle, this could potentially interfere with the decay curve analysis presented in Fig. 4; additional intensity at early times would result in a half-life that is too long. When we corrected the 811-keV photon-intensity data presented in Fig. 4 for the contribution from the direct decay of $^{58}Co^{m}$ (based on the intensity of the 1266-keV photon), the correction was sufficiently small that the refit half-life shortened by only 0.002 h, with no effect on the average value calculated in Sec. III B.

V. SUMMARY

We have studied some of the nuclear decay properties of $^{58}Co^{m}$, a nuclide with applications in oncology, as well as a potential nuclear-forensic signature in nuclear explosion debris. Counting sources were produced by the irradiation of ^{55}Mn with ^{4}He ions and the subsequent radiochemical isolation of the cobalt isotopes. The half-life of $^{58}Co^{m}$ was found to be (8.853 ± 0.023) h, significantly different from the evaluated data in common use today. Through the growth-and-decay relationship and the absolute intensity of the 811-keV photon emitted by $^{58}Co^{g}$, the intensity of the 24.9-keV $M3$ γ ray emitted in the dominant IT decay of $^{58}Co^{m}$ is $(0.0387 \pm 0.0016)\%$. This value is in good agreement with evaluations obtained by measurements of the relative intensities of the γ ray and x rays. We observed a small decay branch for the EC of $^{58}Co^{m}$ to the 2077-keV state in ^{58}Fe, with a partial half-life of 84 years. This is within the log ft range expected for the allowed, ℓ-forbidden transition, and is much less than transitions to other states. Assuming that 100% of the EC decays result in the observed 1266-keV γ-ray transition, the $^{58}Co^{m}$ EC branch is $(0.00120 \pm 0.00005)\%$.

ACKNOWLEDGMENTS

The authors would like to thank the staff of the LLNL Nuclear Counting Facility for their help with γ-ray spectrometry, and the staff of CAMS for irradiation assistance.

This work was performed under the auspices of the U.S. Department of Energy by the Lawrence Livermore National Laboratory under Contract DE-AC52-07NA27344. This work was funded by the Laboratory Directed Research and Development program under tracking code 16-SI-001.

[1] R. G. H. Robertson and R. G. Summers-Gill, Can. J. Phys. **49**, 1186 (1971).
[2] M. H. Brennan and A. M. Bernstein, Phys. Rev. **120**, 927 (1960).
[3] T. Taylor and R. G. Summers-Gill, Can. J. Phys. **56**, 793 (1978).
[4] C. Schwartz, Phys. Rev. **94**, 95 (1954).
[5] K. Strauch, Phys. Rev. **79**, 487 (1950).
[6] J. L. Campbell, R. J. Goble, H. J. Smith, and O. Dragoun, Nucl. Phys. A **152**, 631 (1970).
[7] F. Pleiter, Nucl. Phys. A **163**, 425 (1971).
[8] H.-J. Strutz, Z. Phys. **207**, 119 (1967).
[9] B. Wilken, Z. Phys. **213**, 56 (1968).
[10] P. Bernhardt, E. Forssell-Aronsson, L. Jacobsson, and G. Skarnemark, Acta Oncol. **40**, 602 (2001).
[11] H. Thisgaard, D. R. Elema, and M. Jensen, Med. Phys. **38**, 4535 (2011).
[12] H. Thisgaard, B. B. Olsen, J. H. Dam, P. Bollen, J. Mollenhauer, and P. F. Høilund-Carlsen, J. Nucl. Med. **55**, 1311 (2014).
[13] H. F. Valdovinos, R. Hernandez, S. Graves, P. A. Ellison, T. E. Barnhart, C. P. Theuer, J. W. Engle, W. Cai, and R. J. Nickles, Appl. Radiat. Isot. **130**, 90 (2017).
[14] R. B. Michel, M. W. Brechbiel, and M. J. Mattes, J. Nucl. Med. **44**, 632 (2003).
[15] I. L. Preiss and R. W. Fink, Nucl. Phys. **15**, 326 (1960).
[16] T. Matsuo, J. M. Matuszek, N. D. Dudey, and T. T. Sugihara, Phys. Rev. **139**, B886 (1965).
[17] S. Sudár and S. M. Qaim, Phys. Rev. C **53**, 2885 (1996).
[18] C. M. Buczkó, J. Csikai, S. Sudár, A. Grallert, S. A. Jonah, B. W. Jimba, T. Chimoye, and M. Wagner, Phys. Rev. C **52**, 1940 (1995).
[19] C. D. Nesaraja, S. D. Geraedts, and B. Singh, Nucl. Data Sheets **111**, 897 (2010).
[20] J. J. Livingood and G. T. Seaborg, Phys. Rev. **60**, 913 (1941).
[21] L. S. Cheng, J. L. Dick, and J. D. Kurbatov, Phys. Rev. **88**, 887 (1952).
[22] S. Sudár and S. M. Qaim, Phys. Rev. C **50**, 2408 (1994).
[23] L. Marquez, Phys. Rev. **88**, 225 (1952).
[24] C. J. Avery, K. C. Kaericher, and M. L. Pool, Phys. Rev. **87**, 179 (1952).
[25] S. Sudár, F. Szelecsényi, and S. M. Qaim, Phys. Rev. C **48**, 3115 (1993).
[26] J. C. Davis, Nucl. Instrum. Meth. B **40–41**, 705 (1989).
[27] M. L. Sundquist, J. R. Adney, and R. C. Schmidt, Nucl. Instrum. Meth. B **99**, 684 (1995).
[28] N. Gharibyan, K. J. Moody, S. J. Tumey, T. A. Brown, J. D. Despotopulos, S. A. Faye, K. E. Roberts, and D. A. Shaughnessy, Appl. Radiat. Isot. **107**, 199 (2016).
[29] J. D. Despotopulos, K. N. Kmak, and D. A. Shaughnessy, J. Radioanal. Nucl. Chem. **317**, 985 (2018).
[30] L. C. Northcliffe and R. F. Schilling, At. Data Nucl. Data Tables **7**, 233 (1970).
[31] F. Hubert, A. Fleury, R. Bimbot, and D. Gardes, Ann. Phys. (Paris) **5**, 1 (1980).
[32] M. Wang, G. Audi, F. G. Kondev, W. J. Huang, S. Naimi, and X. Xu, Chin. Phys. C **41**, 030003 (2017).
[33] L. C. Bate and G. W. Leddicote, The Radiochemistry of Cobalt, NAS-NS-3041 (Subcommittee on Radiochemistry, National Academy of Sciences-National Research Council, 1961).
[34] G. F. Knoll, *Radiation Detection and Measurement*, 3rd edn. (John Wiley & Sons, New York, 2000).
[35] R. G. Helmer, R. C. Greenwood, and R. J. Gehrke, Nucl. Instrum. Methods **155**, 189 (1978).
[36] R. C. Greenwood, R. G. Helmer, and R. J. Gehrke, Nucl. Instrum. Methods **159**, 465 (1979).
[37] R. B. Firestone and V. S. Shirley, eds., *Table of Isotopes*, 8th edn. (John Wiley & Sons, New York, 1996).
[38] R. Gunnink and J. B. Niday, Computerized Quantitative Analysis by Gamma Ray Spectrometry, Report UCRL-51061 (Lawrence Livermore Laboratory, 1971).
[39] R. Gunnink and J. B. Niday, in *ERDA Symposium of x- and gamma-ray Sources and Applications* (U.S. Energy Research and Development Administration, CONF-760529, Washington, D.C., GPO, 1976).
[40] E. F. Plechatty, D. E. Cullen, and R. J. Howerton, Tables and Graphs of Photon Interaction Cross Sections from 1.0 keV to 100 MeV Derived from the LLL Evaluated Nuclear Data Library, Report UCRL-50400, Vol. 6 (Lawrence Livermore Laboratory, 1975).
[41] C. M. Davisson, in *Alpha-, Beta- and Gamma-Ray Spectroscopy*, edited by K. Siegbahn (Elsevier, Amsterdam, 1968), Chap. 2.
[42] J. H. Hubbell, Radiat. Res. **70**, 58 (1977).
[43] J. M. Cork, M. K. Brice, and L. C. Schmid, Phys. Rev. **99**, 703 (1955).
[44] U. Reus and W. Westmeier, At. Data Nucl. Data Tables **29**, 1 (1983).
[45] F. F. Dyer and G. W. Leddicote, The Radiochemistry of Copper, NAS-NS-3027 (Subcommittee on Radiochemistry, National Academy of Sciences-National Research Council, 1961).
[46] E. P. Mignonsin, Appl. Radiat. Isot. **45**, 17 (1994).
[47] P. Bevington, *Data Reduction and Error Analysis for the Physical Sciences* (McGraw-Hill, New York, 1969).
[48] K. J. Moody, Ph.D. thesis, University of California, Berkeley, Lawrence Berkeley Laboratory, 1983, Report LBL-16249.
[49] W. M. Good, D. Peaslee, and M. Deutsch, Phys. Rev. **69**, 313 (1946).
[50] H. Daniel, Z. Phys. **150**, 144 (1958).
[51] J. Konijn, H. L. Hagedoorn, H. van Krugten, and J. Slobben, Physica **24**, 931 (1958).
[52] T. Szymanski and M. Thoennessen, At. Data Nucl. Data Tables **96**, 848 (2010).
[53] G. Friedlander, J. W. Kennedy, E. S. Macias, and J. M. Miller, *Nuclear and Radiochemistry*, 3rd edn. (John Wiley & Sons, New York, 1981), Chap. 5.
[54] H. Heylen, C. Babcock, J. Billowes, M. L. Bissell, K. Blaum, P. Campbell, B. Cheal, R. F. Garcia Ruiz, C. Geppert, W. Gins, M. Kowalska, K. Kreim, S. M. Lenzi, I. D. Moore, R. Neugart, G. Neyens, W. Nörtershäuser, J. Papuga, and D. T. Yordanov, Phys. Rev. C **92**, 044311 (2015).
[55] N. C. Dyer and J. H. Hamilton, Nucl. Phys. A **173**, 393 (1971).

[56] K. G. Tirsell, L. G. Multhauf, and S. Raman, Phys. Rev. C **10**, 785 (1974).
[57] D. Christian and D. S. Martin, Jr., Phys. Rev. **80**, 1110 (1950).
[58] D. C. Hoffman and D. S. Martin, Jr., J. Phys. Chem. **56**, 1097 (1952).
[59] C. E. Rhoades, Jr. and H. A. Medicus, Phys. Rev. **167**, 1049 (1968).
[60] B. Grinberg, J. P. Brethon, F. Lagoutine, Y. Le Gallic, J. Legrand, A. H. Wapstra, H. M. Weiss, W. Bambynek, E. De Roost, H. H. Hansen, and A. Spernol (7th Ed.), Atomic Energy Rev. 11 (1973).
[61] L. K. Peker, Nucl. Data Sheets **42**, 457 (1984).
[62] S. Y. F. Chu, L. P. Ekstrom, and R. B. Firestone, "The Lund/LBNL Nuclear Data, Search Version 2.0", Online: http://nucleardata.nuclear.lu.se/toi/, 1999.
[63] M. R. Bhat, Nucl. Data Sheets **80**, 789 (1997).
[64] I. M. Band, M. B. Trzhaskovskaya, C. W. Nestor, Jr., P. O. Tikkanen, and S. Raman, At. Data Nucl. Data Tables **81**, 1 (2002).
[65] A. de-Shalit and H. Feshbach, *Theoretical Nuclear Physics*, Vol. 1: Nuclear Structure (John Wiley & Sons, New York, 1974), Chap. 8.
[66] S. Raman, M. Ertugrul, C. W. Nestor, Jr., and M. B. Trzhaskovskaya, At. Data Nucl. Data Tables **92**, 207 (2006).
[67] R. S. Hager and E. C. Seltzer, Nucl. Data, Sect. A **4**, 1 (1968).
[68] O. Dragoun, H. C. Pauli, and F. Schmutzler, At. Data Nucl. Data Tables **6**, 235 (1969).
[69] T. Kibédi, T. W. Burrows, M. B. Trzhaskovskaya, P. M. Davidson, and C. W. Nestor, Jr., Nucl. Instrum. Meth. A **589**, 202 (2008).
[70] J. Rapaport, A. Trier, T. A. Belote, and W. E. Dorenbusch, Nucl. Phys. A **187**, 25 (1972).
[71] M. J. Schneider and W. W. Daehnick, Phys. Rev. C **5**, 1330 (1972).
[72] H. Nakada and T. Otsuka, Phys. Rev. C **55**, 748 (1997).
[73] D. Steppenbeck, R. V. F. Janssens, S. J. Freeman, M. P. Carpenter, P. Chowdhury, A. N. Deacon, M. Honma, H. Jin, T. Lauritsen, C. J. Lister, J. Meng, J. Peng, D. Seweryniak, J. F. Smith, Y. Sun, S. L. Tabor, B. J. Varley, Y.-C. Yang, S. Q. Zhang, P. W. Zhao, and S. Zhu, Phys. Rev. C **85**, 044316 (2012).
[74] N. B. Gove and M. J. Martin, At. Data Nucl. Data Tables **10**, 205 (1971).
[75] S. Raman and N. B. Gove, Phys. Rev. C **7**, 1995 (1973).
[76] S. A. Moszkowski, in *Alpha-, Beta- and Gamma-Ray Spectroscopy*, edited by K. Siegbahn (Elsevier, Amsterdam, 1968), Chap. 15.